Proceedings of Meetings on Acoustics

NOVEMBER 19 2025

Optimisation of a controllable Helmholtz resonator to achieve high frequency reconfigurability with large absorption values

Yuan Kit Sim ; Felix Langfeldt ; Falk-Martin Hoffmann

Proc. Mtgs. Acoust. 57, 030004 (2025)
https://doi.org/10.1121/2.0002154

Volume 57 http://acousticalsociety.org/

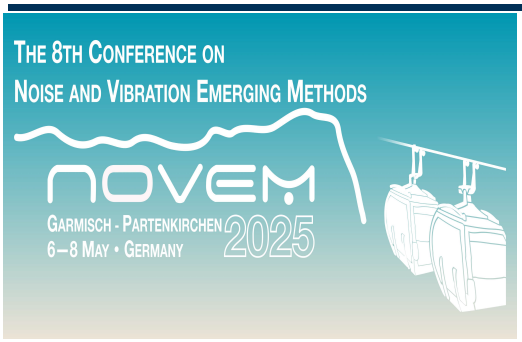

NOVEM2025

NOise and Vibration Emerging Methods

Garmisch-Partenkirchen, Germany

6-8 May 2025

Engineering Acoustics: Noise and Vibration Control

Optimisation of a controllable Helmholtz resonator to achieve high frequency reconfigurability with large absorption values

Yuan Kit Sim and Felix Langfeldt
University of Southampton Institute of Sound and Vibration Research, Southampton, Hampshire, SO17 1BJ, UNITED KINGDOM; Y.K.Sim@soton.ac.uk; F.Langfeldt@soton.ac.uk

Falk-Martin Hoffmann
Sony Europe Limited, Stuttgart, Baden-Württemberg, GERMANY; Falk-Martin.Hoffmann@sony.com

Helmholtz resonators (HR) are effective acoustic absorbers in the low frequency regime, where the performance of conventional porous absorbers is limited. This is evident by their widespread applications, from controlling room modes to reducing noise transmission in ducts and fan noise radiated by aero-engines. However, HR-based sound absorbers only achieve significant sound absorption within a narrow frequency range. Thus, HR can become ineffective as soon as the acoustic environment changes (e.g., when increasing the occupancy of a room) and the problematic frequency falls outside the HR's target frequency range. In response to the dynamically changing acoustic environment, a controllable HR with a large frequency reconfigurability range would be required. Recent research efforts have focused on reconfigurable HR that enable resonance frequency tuning over a large frequency range, but the sound absorption levels of the HR were not considered. In this contribution, a numerical optimisation study of a controllable HR to achieve a high frequency reconfigurability with simultaneously large sound absorption values throughout the reconfiguration range is presented. To achieve reconfigurability, a cylindrical HR with a controllable neck radius is considered and its geometry as well as added layers of porous material in the HR cavity are optimised.

Proceedings of Meetings on Acoustics, Vol. 57, 030004 (2025); https://doi.org/10.1121/2.0002154.

1. INTRODUCTION

Helmholtz resonators (HRs) are highly effective in absorbing sound at low frequencies, where the performance of conventional porous absorbers is limited by their thickness. However, HRs only exhibit significant sound absorption within a narrow operating frequency range around the Helmholtz resonance frequency. This means that HRs become ineffective when a problematic frequency of a changing acoustic environment (e.g., a tonal noise source or a mode in a room) differs from the designed resonance frequency of a HR. For example, such a situation can occur when an aero-engine fan increases its rotational speed and, consequently, its associated blade passing frequency increases. Another example is when a change in occupancy within a room changes the eigenfrequency of a problematic room mode. To mitigate this, controllable HRs (CHRs) with a reconfigurable resonance frequency were proposed, where the reconfigurability is achieved by controlling the geometric parameters of the HR.[1–5]

Recent research efforts have focused on controlling the volume of the HR cavity, e.g. by geometrically adjusting the cavity height of the HR,[4,5] as a means of reconfiguring the resonance frequency. The advantage of changing the cavity volume is that this does not significantly affect the acoustic resistance (and, consequently, the impedance matching) of the HR and hence a consistently high absorption coefficient can be achieved throughout the reconfiguration range. However, with the aim of achieving a large frequency reconfigurability range, controlling the geometry of the HR neck (e.g., using an iris mechanism for a cylindrical neck[6,7]) may be more effective. This can simply be demonstrated with the resonance frequency equation for a HR with a cylindrical neck and cavity

$$f_\mathrm{r} = \frac{c_0}{2\pi}\sqrt{\frac{\pi a_1^2}{l_1 \cdot \pi R_1^2 H_1}} = \frac{c_0}{2\pi}\frac{a_1}{R_1}\sqrt{\frac{1}{l_1 H_1}}, \tag{1}$$

where c_0 is the speed of sound, a_1 is the neck radius, l_1 is the (effective) neck length, R_1 is the cavity radius, and H_1 is the cavity height. According to Eq. (1), a twofold increase of a_1 raises the resonance frequency of the HR by a factor of two, whereas a twofold reduction of H_1 only raises the resonance frequency by a factor of $\sqrt{2}$. Given that the resonance frequency of a HR appears to be equally sensitive to both a_1 and $1/R_1$, one may choose to reconfigure the resonance frequency by controlling the radius of the HR cavity. However, considering that the geometrical dimension of the neck is always substantially smaller than the cavity in a HR, controlling the neck radius can lead to higher (relative) resonance frequency changes for the same (absolute) geometrical change. This approach would require the least amount of actuation, which may be critical for an efficient adaptation of an array of CHR to a changing acoustic environment. However, since changing the neck radius affects the resistance of a HR, a change in the neck radius would lead to a change in the absorption coefficient. This could mean that despite a high frequency reconfigurability range, a CHR with an adjustable neck radius may suffer from a strongly reduced sound absorption within large parts of this frequency range, due to over- or underdamping.

To address this problem, in this contribution, a numerical optimisation method for a CHR is presented. This optimisation method is designed to achieve a CHR with a large frequency reconfigurability range, with particular attention given to maintain or enhance its absorption performance within the frequency reconfigurability range, despite possible changes in resistance due to a changing neck radius. This paper is structured as follows: Section 2 describes the geometrical parameters of the CHR considered here, and the numerical model used to compute its sound absorption, as well as the formal definition of the optimisation problem. Then, Section 3 presents and discusses the optimisation results for three cases: a CHR with cavity height change, a CHR with neck radius change, and a CHR with neck radius change and an added layer of porous material inside the cavity. The key findings of this paper are summarised in Section 4.

2. METHODOLOGY

This section first describes the general design of the CHR considered here and explains the numerical modelling approach used for calculating its sound absorption coefficient α. Using this numerical model, three optimisation cases are considered: As a benchmark, the cavity height of the CHR is controlled in case I. The neck radius is chosen as the controllable parameter in case II. In optimisation case III, the neck radius remains as the controllable parameter. However, to compensate for the reduction in resistance when the neck radius increases, a similar approach to Ref. 6 is taken, where an additional porous layer is added onto the base of the HR cavity. The formal definition of the optimisation problem for these cases is provided at the end of this section, including an objective function and the constraints that consider both the frequency reconfigurability range and the minimum target sound absorption coefficient within this range.

A. CHR DESIGN AND NUMERICAL MODEL

The geometry of the cylindrical HR considered here is defined in an axisymmetric cylindrical coordinate system, as shown in Fig. 1. The geometry of the HR is given by the neck length l_1, neck radius a_1, cavity radius R_1, and cavity height H_1. The neck of the resonator is connected to a circular duct with radius R_{air}. In the optimisation setup (which will be described later), the cavity radius R_1 is expressed as a product of the duct radius R_{air} and a scaling factor S_{R}. Similarly, the neck radius a_1 is expressed as a product of the cavity radius R_1 and a scaling factor S_{a}, which has to be positive but less than one so that the neck radius is smaller than the cavity radius.

The CHR is placed at the end of a circular duct and is excited by a plane acoustic wave that is normally incident on the CHR. As shown in Fig. 1, the resonator is modelled using an axisymmetric numerical model based on the finite element method (FEM), with the fluid material being air (density $\rho_0 = 1.2\,\mathrm{kg\,m^{-3}}$ and speed of sound $c_0 = 343\,\mathrm{m\,s^{-1}}$). The incident side of the circular duct is terminated using a non-reflecting boundary condition. To account for the thermoviscous losses in the CHR (especially within the neck), the sound field within the CHR and close to its top boundary (as represented by the orange region in Fig. 1) is modelled using the linearised Navier-Stokes equations. The wall boundaries in this domain are modelled as isothermal no-slip walls, leading to thermoviscous losses at these boundaries. As negligible dissipation is expected to occur in the incident fluid domain (represented by the green region in Fig. 1), the fluid in this domain is assumed to be inviscid and adiabatic to improve computational efficiency. For the third optimisation case (where a porous layer is added to the CHR cavity), the porous layer (represented by the pink region in Fig. 1) is assumed to be rock wool and is modelled using the limp formulation of the Johnson-Champoux-Allard (JCA) equivalent fluid model.[8] The corresponding properties required for the JCA model, porosity ϵ, flow resistivity σ, thermal characteristic length L_{th}, viscous characteristic length L_{v}, tortuosity factor τ, and bulk density ρ, are summarised in Table 1.

Figure 1 also shows the mesh that was used to discretise the numerical model with the FEM. The maximum element size in the CHR neck was set to $\min(a_1, \frac{c_0}{f_{\max}})/5$, where $f_{\max} = 1200$ Hz is the maximum frequency of interest, so that at least five elements per wavelength or neck radius are present in the discretised FEM model. Particular care was also given to resolve the thermoviscous boundary layers in the neck and cavity, by using a six-layer boundary layer mesh with a total thickness equal to the viscous boundary layer

Table 1: The JCA model parameters used to represent the rock wool material in the simulations.[8]

Parameter	ϵ	σ	L_{th}	L_{v}	τ	ρ
Value	0.94	135000	166	49	2.1	130
		$\mathrm{Pa\,s\,m^{-2}}$	µm	µm		$\mathrm{kg\,m^{-3}}$

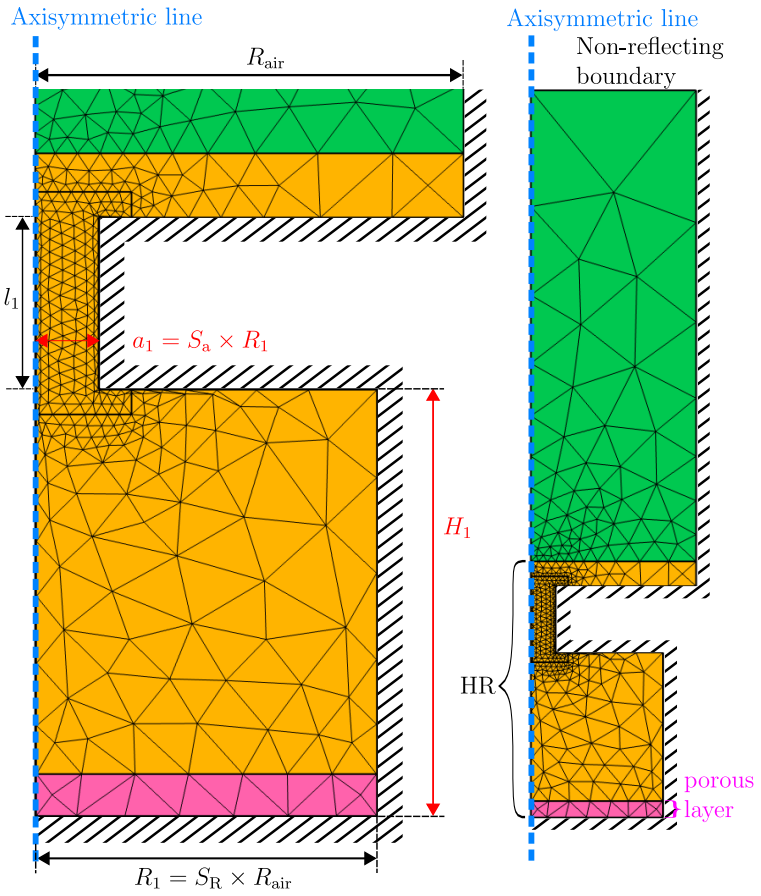

Figure 1: Finite element model of the CHR and its key geometrical dimensions. Left: close view of the CHR; Right: overview of the whole numerical model.

thickness (considering that for air, the viscous boundary layer is always thinner than the thermal boundary layer). To calculate the sound absorption coefficient α of the CHR, the simulations were performed in the frequency domain (frequency range: 100 to 1200 Hz). At each simulated frequency f, the amplitudes of the incident and reflected sound wave, p_{in} and p_{re}, respectively, were extracted from the FEM results to calculate α according to

$$\alpha = 1 - \left| \frac{p_{\text{re}}}{p_{\text{in}}} \right|^2 . \tag{2}$$

B. OPTIMISATION METHOD

Table 2 provides an overview of the range of the geometrical control parameters (corresponding to the displacement range of the corresponding control actuators) in each optimisation case. This means, for example, that the neck radius is increased from 2 mm to 6 mm regardless of the geometry of the CHR. In a practical scenario, this corresponds to a particular choice of actuation mechanism that provides this fixed range of actuation to achieve the frequency reconfigurability. For a better comparability between controlling H_1 (in case I) and a_1 (in cases II and III), both control parameters are varied by the same relative factor of three. The minimum and maximum allowable thickness (i.e., $l_1 + H_1$) of the CHR are set to be 12 mm and 40 mm, respectively.

In optimisation case I, the geometrical parameters of the CHR are optimised according to the following

Table 2: The range of the control parameters and the weighting factors used for each optimisation case.

Case	Control parameter	Range	w_1	w_2
I	H_1	24 - 8 mm	0.85	0.15
II	a_1	2 - 6 mm	0.95	0.05
III	a_1	2 - 6 mm	0.95	0.05

optimisation problem statement:

$$\begin{aligned} \underset{S_\mathrm{a},\, S_\mathrm{R},\, R_\mathrm{air},\, l_1}{\text{minimize}} \quad & w_1 \left| \frac{f_\mathrm{L} - f_\mathrm{L,desired}}{0.1 f_\mathrm{max}} \right| - w_2 \frac{f_\mathrm{U} - f_\mathrm{L}}{\sqrt{f_\mathrm{U} f_\mathrm{L}}} \\ \text{subject to} \quad & \alpha_\mathrm{L} \geq 0.8, \\ & \alpha_\mathrm{U} \geq 0.8, \\ & S_\mathrm{a} \in [0.05, 0.15]\,, \\ & S_\mathrm{R} \in [0.5, 1.0]\,, \\ & R_\mathrm{air} \in [20\ \mathrm{mm}, 50\ \mathrm{mm}]\,, \\ & l_1 \in [4\ \mathrm{mm}, 16\ \mathrm{mm}]\,. \end{aligned} \tag{3}$$

To explain the terms used in the optimisation problem statement, the sound absorption curves of a non-optimised example CHR design, with H_1 varying from 24 mm to 8 mm, are shown in Fig. 2. As illustrated in Fig. 2, f_L and f_U denote the resonance frequencies at the lower and upper limit of the control

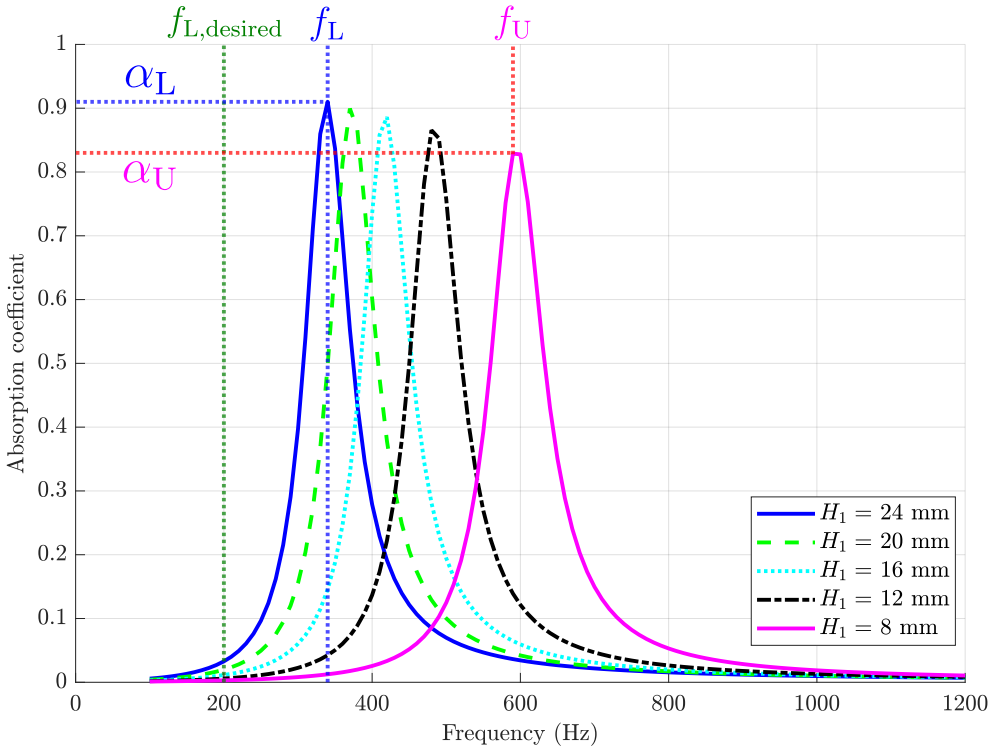

Figure 2: Sound absorption curves of a non-optimised example CHR design for different values of the cavity height H_1.

parameter range, respectively. α_{L} and α_{U} denote the respective absorption coefficients at these frequencies. Additionally it can be seen that since the intermediate resonance peaks (corresponding to $H_1 = 20\ \mathrm{mm}$, $16\ \mathrm{mm}$, $12\ \mathrm{mm}$) must occur between f_{L} and f_{U}, they also have peak absorption coefficient values between α_{L} and α_{U}. Thus, these intermediate states of the CHR are not considered in the simulation and optimisation procedure, inherently reducing the computational effort.

The objective function is composed of two objectives weighted using w_1 and w_2: The first objective aims to minimise the difference between f_{L} and the desired lower target frequency, $f_{\mathrm{L,desired}} = 200\ \mathrm{Hz}$. The second objective function aims at maximising (hence the minus sign in front of w_2) the frequency reconfigurability range, which is defined as the relative bandwidth (based on the frequency difference between the two peaks at f_{L} and f_{U}, respectively). It should be noted that the relative bandwidth tends to be in the order of one. Therefore, to facilitate an approximately equal magnitude for the two objectives, the first objective is normalised using $f_{\max}/10 = 120\ \mathrm{Hz}$. For the same reason, considering that the frequency reconfigurability range is expected to be larger when a_1 is controlled (than when H_1 is controlled), the first objective has a slightly higher relative weighting (i.e., $w_1 = 0.95$) in optimisation cases II and III than in optimisation case I. Another important aspect of the optimisation statement is to ensure that the CHR achieves a certain minimum sound absorption value throughout its reconfigurability range. This is implemented using the inequality constraints, which require both α_{L} and α_{U} to be at least 0.8. Based on the discussion above, this also ensures that the peak sound absorption coefficient will be at least 0.8 in all intermediate reconfigurability states. For better convergence, all design variables are normalised to parameter ranges between 0 and 1 in the optimisation algorithm implementation.

In the optimisation cases II and III (where the neck radius is varied), a_1 is fixed in the range of 2 to 6 mm and the design variable S_{a} in Eq. (3) is replaced by $H_1 \in [8\ \mathrm{mm}, 24\ \mathrm{mm}]$. An additional design variable, $S_{\mathrm{porous}} \in [0.05, 0.5]$ (i.e., the ratio of the thickness of the porous layer to the cavity height) is also included in the optimisation case III. The optimisation problem is then solved using MATLAB's `fmincon` function,[9] which is a non-linear constrained gradient-based optimiser that employs the interior-point algorithm to find a local minimum, with the gradients of the objective function being computed using the finite difference method. To increase the likelihood that the optimisation algorithm converges towards the global minimum, the optimisation problem is repeated 20 times with random initial variables chosen within the defined bounds. The result with the smallest objective function value (from these 20 repetitions) is then chosen, provided that the result does not violate the inequality constraints (that require both α_{L} and α_{U} to be at least 0.8).

3. RESULTS AND DISCUSSION

The geometrical parameters of the optimised CHR designs for each of the three optimisation cases are tabulated in Table 3. Table 4 shows the values of the resulting upper and lower frequencies of the reconfigurability range as well as the values of the two objectives. The corresponding sound absorption coefficient curves of the optimised CHR and an illustration of the dimensional changes due to the actuation are shown in Fig. 3 and Fig. 4, respectively. As tabulated in Table 4 and shown in Fig. 3, the cases I and III resulted in the first resonance peak occurring at the desired lower target frequency $f_{\mathrm{L,desired}} = 200\ \mathrm{Hz}$, whereas a difference of 40 Hz is observed in case II. A discussion of the results for each specific optimisation case follows in the subsequent sections.

A. OPTIMISATION CASE I

As shown in Fig. 3, reducing the cavity height from 24 mm to 8 mm shifts the CHR resonance peak up in frequency from 200 Hz to 350 Hz, which is equivalent to a relative bandwidth of 0.57. It is also worth noting that $\alpha \geq 0.9$ is achieved at both peaks, with near-perfect absorption achieved at f_{L}. This can

Table 3: The optimised geometrical parameters of the CHR for each optimisation case.

Case	Control parameter	H_1	S_a	S_R	R_air	l_1	S_porous
I	H_1	—	0.07	0.90	35.0	10.1	—
II	a_1	8.4	—	0.94	50.0	6.9	—
III	a_1	21.1	—	0.93	28.6	12.7	0.43
		mm			mm	mm	

Table 4: The reconfigurability ranges and objective values of the optimised CHR for each optimisation case.

Case	Control parameter	f_L	f_U	$f_\mathrm{L} - f_\mathrm{L,desired}$	$\frac{f_\mathrm{L}-f_\mathrm{L,desired}}{0.1 f_\mathrm{max}}$	$\frac{f_\mathrm{U}-f_\mathrm{L}}{\sqrt{f_\mathrm{U} f_\mathrm{L}}}$
I	H_1	200	350	0	0	0.57
II	a_1	240	590	40	0.33	0.93
III	a_1	200	570	0	0	1.10
		Hz	Hz	Hz		

be attributed to the changes of the cavity volume not significantly affecting the resistance of CHR, as the thermal dissipation in the cavity typically is significantly smaller than the viscous dissipation in the neck. The optimised CHR geometry also has a large ratio of cavity radius to the duct radius (i.e., $S_\mathrm{R} = 0.90$). This aligns with the expectation that the volumetric change in the cavity (for a given cavity height change ranging from 24 mm to 8 mm) can be maximised by increasing the lateral dimensions of the cavity, such that a large resonance peak shift can be achieved.

B. OPTIMISATION CASE II

When varying the neck radius from $a_1 = 2$ mm to 6 mm, the optimised CHR design in case II leads to a 63% increase of the relative reconfigurability bandwidth compared to case I (i.e., from 0.57 to 0.93). Despite the change in a_1, which is expected to have a more significant influence on the acoustic resistance (than changing H_1), once optimised, a minimum $\alpha = 0.8$ is achieved throughout the reconfiguration range. Further investigation of the acoustic impedance of the CHR (not shown) reveals that the resonance peaks at f_L and f_U are overdamped and underdamped, respectively. This is also reflected by the presented optimisation result, where the optimised CHR design in case II has the largest duct radius (among all three cases) to improve the impedance matching between the underdamped CHR and the background air medium, in order to raise α_U to 0.8.

It can be seen in Fig. 4 that the optimised CHR design in case II has the smallest cavity height, which suggests that the effect of viscous and thermal dissipation in the cavity becomes more significant, albeit not to the extent of the viscous dissipation in the neck.[10] Also, the optimised CHR design has the shortest neck length. These are likely to reduce the dependency of the acoustic resistance on the CHR neck, such that increasing the neck radius does not yield as much reduction in the acoustic resistance, and hence the absorption coefficient can be maintained.

Unlike optimisation cases I and III, the first resonance peak occurs at $f_\mathrm{L} = 240$ Hz, instead of the desired lower target frequency $f_\mathrm{L,desired} = 200$ Hz. Inspection of the rejected optimisation results (which resulted from different initial points) suggests that a minimum $f_\mathrm{L} - f_\mathrm{L,desired} = 0$ Hz is achieved only when the inequality constraints (i.e., $\alpha_\mathrm{L} \geq 0.8$, $\alpha_\mathrm{u} \geq 0.8$) are violated. Therefore, for a more accurate and less restrictive optimisation with better convergence, the controllable parameter, instead of being fixed, also needs to be optimised within the bound that corresponds to the geometrical actuation range (of the actuation

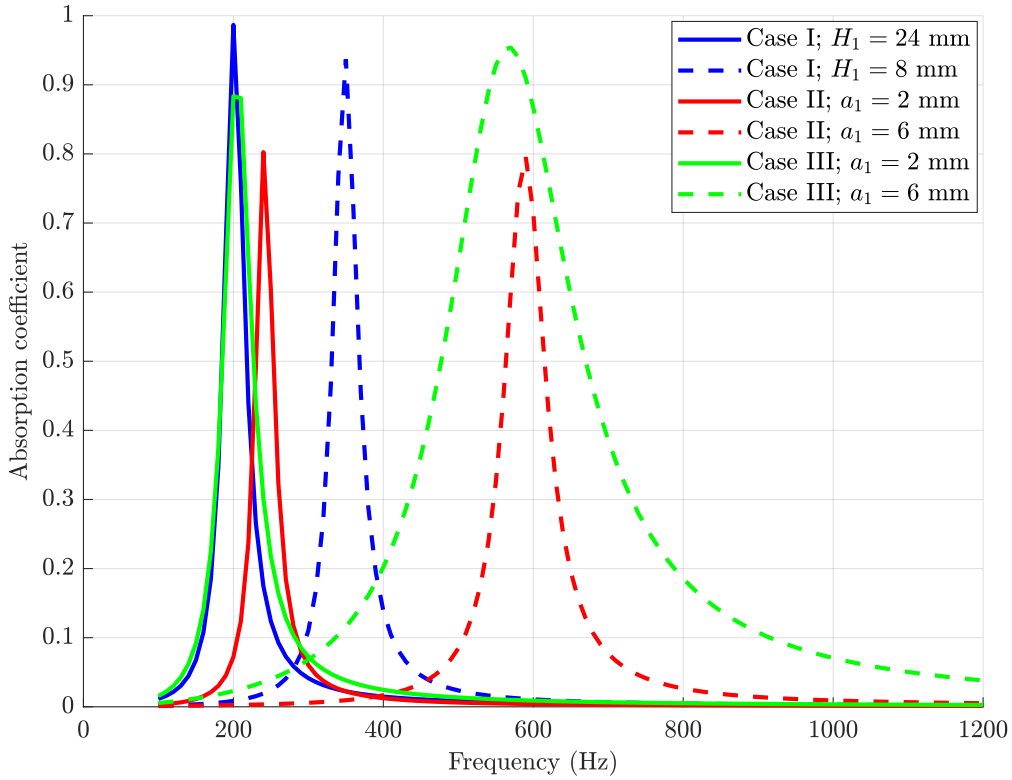

Figure 3: Sound absorption coefficient of the three optimised CHR designs. In all three cases, the solid lines correspond to the absorption curves at the lower limit of the reconfiguration range, whereas the dashed lines correspond to the absorption curves at the upper limit of the reconfiguration range.

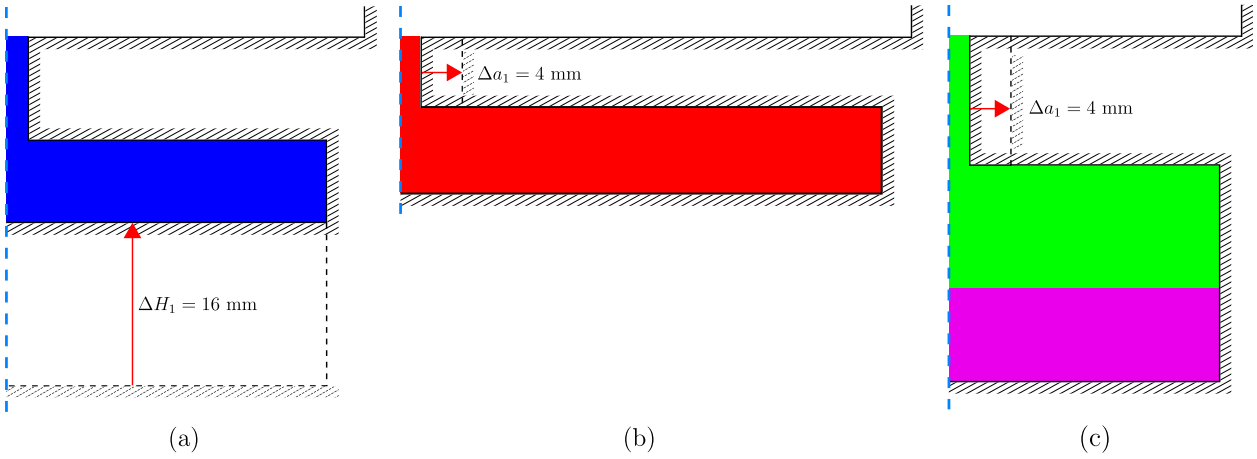

Figure 4: True to scale illustration of the geometry of the respective optimised CHR design in optimisation cases (a) I, (b) II and (c) III. The red arrows denote the directional change of the respective controllable parameter to shift the CHR resonance up in frequency.

mechanism used). Overall, it can be deduced that the best CHR design with a controllable neck radius should have an optimally overdamped characteristic at f_{L} and an optimally underdamped characteristic at f_{U}. In other words, the best CHR design optimised for the largest achievable frequency reconfigurability range should exhibit the lowest possible α_{L} and α_{U} (without violating the absorption constraints).

C. OPTIMISATION CASE III

The layer of rock wool with thickness $S_{\mathrm{porous}} \cdot H_1$ added onto the base of the cavity allows for a compensation of the reduction of resistance (when the neck enlarges). Although this is not clearly shown in Fig. 3 (since the optimised CHR design in case II has achieved a minimum $\alpha = 0.8$ throughout the reconfiguration range), this is evident from the significantly higher absorption coefficient achieved by the optimised CHR design in case III. In terms of the reconfigurability range, the relative bandwidth of the optimised CHR has significantly improved from 0.93 in case II to 1.10, which is almost doubling the relative bandwidth achieved in case I. The bandwidth of the individual resonance peaks, especially at f_{U}, also appears to be broader, due to the greater damping provided by the porous material. It should be noted that the range of a_1 for reconfiguration is fixed in this work. Since α_{U} is much larger than 0.8 in this case, it can be expected that the frequency reconfigurability range could be even larger if a higher upper limit of a_1 was allowed.

4. CONCLUSION

In this work, a numerical optimisation on a space-constrained controllable cylindrical Helmholtz resonator was conducted with the objective to widen its frequency reconfigurability range, while maintaining an acceptable level of absorption (i.e., $\alpha \geq 0.8$) throughout the reconfiguration range. A common method to realise a CHR with such properties is by controlling the cavity height of a HR, but here we investigated the possibility of changing the HR neck radius instead, leading to a possibly higher reconfigurability. Three optimisation cases with different control parameters were considered: case I, where the cavity height was controlled, and cases II and III, where the neck radius was controlled, with an additional porous layer being added onto the base of the cavity in case III. By assuming a fixed range for the control parameters (i.e., $8\ \mathrm{mm} \leq H_1 \leq 24\ \mathrm{mm}$ and $2\ \mathrm{mm} \leq a_1 \leq 6\ \mathrm{mm}$), we could show that an optimised CHR with much larger frequency reconfigurability range can be achieved with a significantly smaller geometrical actuation range by controlling the neck radius (as compared to controlling the cavity height). However, as the neck radius increases, the CHR inevitably suffers from a significant reduction of resistance, and hence its absorption performance can be compromised. Our optimisation procedure could demonstrate that such an issue can be mitigated, with an acceptable level of absorption maintained throughout the reconfiguration range, but at the cost of not fully achieving the frequency target for the lower boundary of the reconfigurable frequency range. Alternatively, the addition of a porous layer with an optimised thickness in the cavity solves this problem by providing additional resistance to the underdamped resonator at large neck radii.

Building on the results presented in this conference contribution, future work can investigate alternative statements of the optimisation problem, e.g. by allowing an optimisation of the range of the control parameters, which is expected to further increase the achievable reconfigurability range. Furthermore, the physical implementation of the actuation mechanism to achieve a change in the neck radius has been neglected in this work. Thus, the next steps in this research will also involve the design of actuation methods to achieve the predicted reconfigurability ranges and test the proposed CHR within an experimental setup.

ACKNOWLEDGMENTS

The authors acknowledge the use of the IRIDIS High Performance Computing Facility, and associated support services at the University of Southampton, in the completion of this work.

REFERENCES

[1] H. Zhang, Q. Wang, M. Fink, and G. Ma, "Optimizing multi-user indoor sound communications with acoustic reconfigurable metasurfaces," **15**(1), 1–10.

[2] Z. Chen, Y. B. Chong, K. M. Lim, and H. P. Lee, "Reconfigurable 3D printed acoustic metamaterial chamber for sound insulation," **266**, 108978.

[3] C. Yu, X. Chen, M. Duan, M. Li, X. Wang, Y. Mao, L. Zhao, F. Xin, and T. J. Lu, "Adjustable sound absorbing metastructures for low-frequency variable discrete sources," **267**, 108965.

[4] G. Wen, S. Zhang, H. Wang, Z.-P. Wang, J. He, Z. Chen, J. Liu, and Y. M. Xie, "Origami-based acoustic metamaterial for tunable and broadband sound attenuation," **239**, 107872.

[5] X. Xiang, H. Tian, Y. Huang, X. Wu, and W. Wen, "Manually tunable ventilated metamaterial absorbers," **118**(5), 053504.

[6] S. J. Estève and M. E. Johnson, "Adaptive Helmholtz resonators and passive vibration absorbers for cylinder interior noise control," **288**(4–5), 1105–1130.

[7] D. Zhao and A. Morgans, "Tuned passive control of combustion instabilities using multiple Helmholtz resonators," **320**(4–5), 744–757.

[8] J.-F. Allard and N. Atalla, *Propagation of Sound in Porous Media: Modelling Sound Absorbing Materials*, 2nd ed ed. (Wiley).

[9] The MathWorks, Inc., "Optimization Toolbox" .

[10] N. Dickey and A. Selamet, "HELMHOLTZ RESONATORS: ONE-DIMENSIONAL LIMIT FOR SMALL CAVITY LENGTH-TO-DIAMETER RATIOS," **195**(3), 512–517.